1-5. Curved Flow; Circulation; Theory of Lift; Airfoils

In developing the so-called circulation theory of lift it is convenient to introduce a very simple type of flow, namely, the steady, two-dimensional motion of a perfect fluid in concentric circles, the Bernoulli constant having the same value throughout the fluid. For such a flow the streamlines will obviously constitute a family of concentric circles. For purposes of visualization it is convenient to consider one of these streamlines as coinciding with a circular cylinder so that the flow is taken as occurring around the outside of such a cylinder (Fig. 1·21). Consider the equilibrium of a very small element at a distance r from

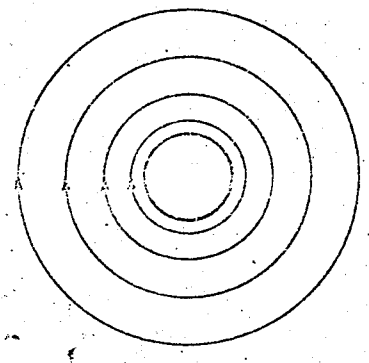

FIG. 1·21. Streamlines for concentric circle flow.

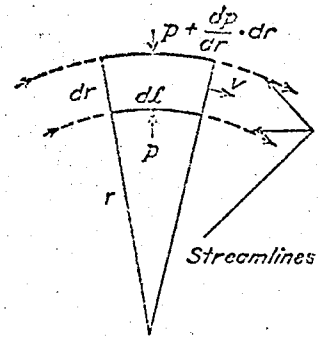

FIG. 1·22. Volume element for the flow of Fig. 1·21.

he center of curvature (Fig. 1·22). The centrifugal force on the fluid e the element must be just balanced by the resultant force due to ressures over the surface. Considering the element to have unit hickness perpendicular to the diagram the volume is $dldr$ and the centrifugal force is $\rho dldr \cdot v^2/r$. The resultant pressure force acting towards he center of curvature * is

$$\left(p + \frac{dp}{dr}\,dr\right)dl - p\,dl = \frac{dp}{dr}\,dr\,dl$$

Equating these forces and canceling $drdl$ we obtain

$$\frac{dp}{dr} = \frac{\rho v^2}{r}$$

* A more accurate analysis taking into account the pressures over the radial faces s shown for Figs. 1·17 and 1·18, leads to exactly the same results.

Now from equation 1·10, or more directly from the equation preceding 1·10, we have, since B is taken as constant throughout the fluid,

$$dp = -\rho v dv$$

Hence

$$-\rho v \frac{dv}{dr} = \frac{\rho v^2}{r}$$

or

$$\frac{dv}{v} = -\frac{dr}{r}$$

and integrating

$$\log v = -\log r + \text{constant}$$

Therefore

$$\log v + \log r = \text{constant}$$

$$\log vr = \text{constant}$$

$$v = \frac{\text{constant}}{r} \qquad [1\cdot14]$$

Hence it has been proved that in such a flow as that which has been considered the velocity is inversely proportional to the radius of curvature of the streamline, i.e., to the distance from the center of the flow. The streamlines of Fig. 1·21 have been drawn so that their spacing indicates this decrease in velocity with increasing radius.

If such a flow existed around a point in the fluid itself rather than around a cylinder, then as $r \to 0$, $v \to \infty$. The point $r = 0$ has therefore very peculiar properties and is called a singular point or in hydrodynamics, a vortex. The circulatory flow around such a vortex is often called a vortex flow and is of fundamental importance in aerodynamics. Since infinite velocities cannot exist in reality, the vortex point must either be a fictitious one lying outside the fluid as in the example of Fig. 1·21, or if it lies in the fluid the conditions in the neighborhood of $r = 0$ must be different from those corresponding to equation 1·14. When vortices do occur in a fluid they are called free vortices and it is found that the effect of viscosity (which was neglected in deriving equation 1·14) is such as to cause the portion of fluid near $r = 0$ to rotate like a solid body with $v \propto r$. Outside of this central core, which is called the vortex core, is a transition region, and outside of this the fluid rotates in accordance with equation 1·14.

By applying Bernoulli's equation with constant total pressure to such a free vortex flow it is seen that the static pressure decreases rapidly towards the center as is shown in the diagram of Fig. 1·23. If the vortex

as considerable intensity and the core has a small diameter, extremely igh suctions can occur in the core. The tornado and waterspout are riking examples of the occurrence in nature of vortex flows with just ese properties. Later, it will be seen that every airplane in flight also ails behind it similar vortex flows whose effects, although less catastrophic than those of the examples just cited, are still very unpleasant.

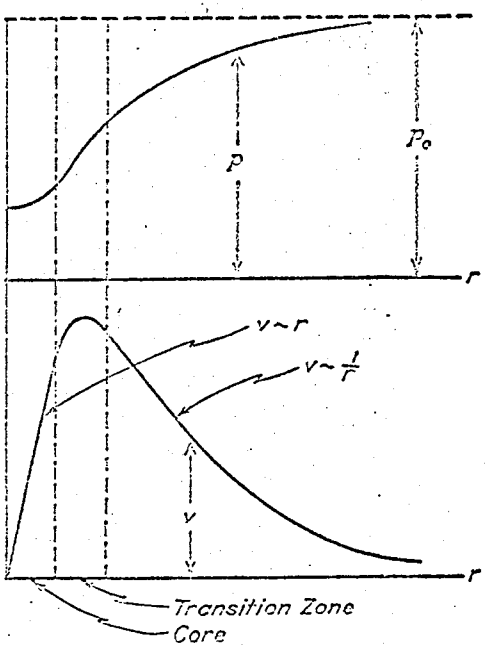

FIG. 1·23. Pressure and velocity distribution in a vortex flow.

In order to generalize some of the characteristics found above to less specialized flows, it is necessary to introduce the conception of circulation. This has a very precise mathematical definition which will first be stated for the benefit of readers with mathematical training. A detailed explanation will then be attempted for those without such training. Consider a given closed path drawn through a region filled with moving fluid. Let v be the fluid velocity at any point along the path, dl be an element of length along the path, and θ the angle between v and dl (Fig. 1·24). Then the circulation, written as Γ, around the given path or contour is the line integral of v os θ around the path, or using the conventional mathematical notation

$$\Gamma = \oint v \cos\theta \, dl \qquad [1\cdot15]$$

It is easy to see what this means by recalling that integration is sentially nothing more than a process of summation. Let us approxiate to our closed path by a polygon of n sides, the lengths of which are $_1$, Δl_2, $\cdots$ Δl_n. Let the fluid velocity at the center of each side be , v_2, $\cdots$ v_n, and the angles between the corresponding v's and l's be , θ_2 $\cdots$ θ_n (cf. Figs. 1·24 and 1·25). Now consider the sum

$$v_1 \cos\theta_1 \, \Delta l_1 + v_2 \cos\theta_2 \, \Delta l_2 + \cdots v_n \cos\theta_n \, \Delta l_n = \Sigma v_i \cos\theta_i \, \Delta l_i$$

obtained by multiplying each length by the tangential component of the velocity at its center and adding all the products together. Now let the number of subdivisions increase while their lengths decrease; then the "line integral" of equation 1·15 is just what is obtained if the limit $n \to \infty$ is approached while the length of each $\Delta l \to dl \to 0$. The word "line" modifying "integral" means that the whole procedure and the integral itself are only defined if a particular path or line is specified along which the summation or integration is carried out.

In order to make this a little clearer let us calculate, as an example, the circulation around one of the circular streamlines of the flow of

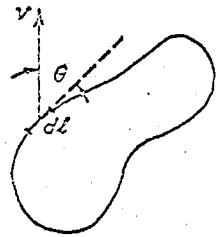

FIG. 1·24. Velocity at a line element.

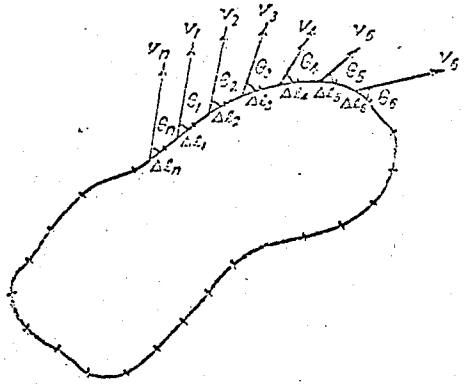

FIG. 1·25. Elementary components of circulation.

Fig. 1·21. Remember that the velocity is everywhere tangential to such a path and its magnitude at any point is given by equation 1·14 which is rewritten

$$v = \frac{A}{r} \qquad [1\cdot16]$$

giving the constant of equation 1·14 the symbol A. Since the velocity is everywhere tangential to the chosen path (cf. Fig. 1·26), θ is everywhere 0 and $\cos\theta = 1$. If we let $d\varphi$ be the central angle subtended by the path element dl, then

$$dl = r\,d\varphi$$

Hence equation 1·15 becomes

$$\Gamma = \oint v \cdot 1 \cdot r\,d\varphi = \oint \frac{A}{r} r\,d\varphi = \oint A\,d\varphi$$

introducing the expression (1·16) for v. The symbol crossing the integral sign indicates the adoption of the convention that the integration is to

e carried out in a clockwise direction around the contour, i.e., from an rbitrary value of φ, say φ_1, to $\varphi_1 + 2\pi$. Since A is constant, inde-endent of φ

$$\Gamma = A \oint d\varphi = A \int_{\varphi_1}^{\varphi_1+2\pi} d\varphi = A\,[(\varphi_1 + 2\pi) - \varphi_1] = 2\pi A \quad [1\cdot17]$$

In this especially simple case the result could have been obtained ithout any integration for, since the tangential component of velocity

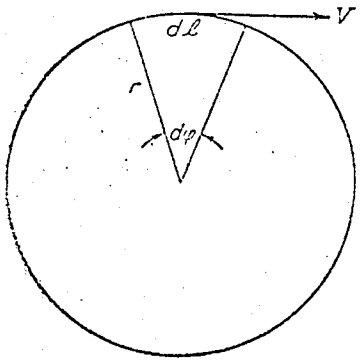

FIG. 1·26. Diagram for circulation with concentric circle flow.

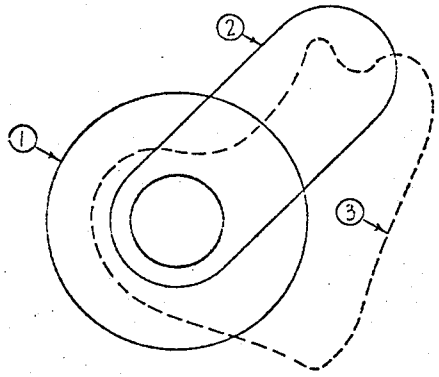

FIG. 1·27. Alternative paths having the same circulation.

$\cos\theta = v = A/r$ is the same for every point on the path, Γ reduces to e simple product of this velocity times the length of path or

$$\Gamma = \left(\frac{A}{r}\right) 2\pi r = 2\pi A$$

A very remarkable fact appears in the result given by equation 1·17 hich is that the magnitude of the circulation is independent of the stance r, i.e., Γ is the same no matter which of the circular streamlines utside the body of Fig. 1·21 we choose for the path of integration. A ill more remarkable result can be rigorously proved, although the oof lies outside the limits of the present discussion; namely, for the w in question the circulation Γ has the same value for every closed th which encloses the cylinder just once, e.g., paths 1, 2, and 3 of g. 1·27. The final generalization which is proved in texts on hydro-namic theory, and which gives a fundamental importance to the con-ption of circulation may be roughly stated in the form: "In a perfect id with constant total pressure the circulation is identical around

simple closed Path

every simple * closed path enclosing a given set of solid bodies or vortices."

This fundamental theorem has as a consequence the fact that the phrase "the circulation around a body" has a unique and well-defined meaning, independent of the choice which may be made of the particular path used for calculating the value of the circulation.

One more conception is required before the above considerations can be applied to the problem of lift which is the objective of the present section. This is the principle of superposition which states that it is possible to build up complex flows by the superposition or addition of a number of simpler flows. In making this addition it must be remembered that the fundamental quantities to be added are velocities, so that the addition must be a vectorial, and not a scalar one. The problem is exactly the same as that of finding the resultant of several forces by adding the various components vectorially. In considering the flow superposition, the velocity vectors of the component flows must be added vectorially at every point to obtain the final resultant or composite flow. As an example, the superposition of a flow with uniform horizontal velocity and another with uniform and equal vertical velocity gives a resultant flow with uniform velocity whose direction is inclined at 45° to the horizontal and whose magnitude is $\sqrt{2}$ times that of the two component flows. Figure 1·28 illustrates the vectorial addition which must be carried out at every point of the flow when such a superposition is made.

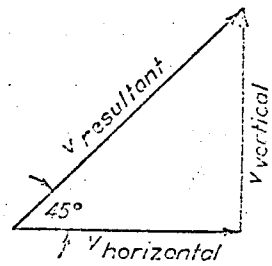

FIG. 1·28. Vectorial addition of component flow velocities.

Figure 1·29 shows velocity vectors and the corresponding streamline patterns for three flows around a circular cylinder. The first is a rectilinear flow with velocity V from left to right which has zero circulation. The fact that the circulation vanishes can be seen by choosing a circular path of integration concentric with the circle and by remembering that for every point above the horizontal line of symmetry there is a symmetrical point below. For the point on top the tangential velocity is in the direction of integration (clockwise), while for that on the bottom it has the same magnitude but is opposite to the direction of integration. Hence $v \cos\theta\, d\ell$ has equal and opposite values for the two symmetrical points so that the corresponding terms cancel when the integration (or

* The word "simple" means primarily that none of the paths compared has a loop so that one or more of the bodies or vortices is passed around more than once in making a single circuit of the path.

summation) is carried out. The entire integration is made up of such pairs of equal and opposite terms so that the final Γ is zero. The second flow is a pure circulatory flow with circular streamlines. It has a circulation, Γ, but no net rectilinear flow. The third is the compound flow

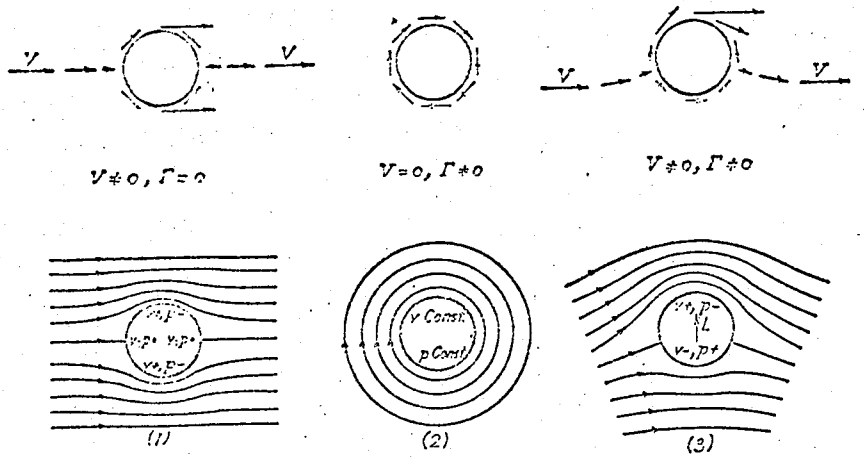

FIG. 1·29. Perfect fluid flows around a circular cylinder.

obtained by superimposing the other two. It has both a rectilinear velocity V and a circulation Γ. In order to avoid confusion only a few velocity vectors are indicated in Fig. 1·29, but enough appear to show the effect of the vector summation involved in the superposition. The streamline pattern can be deduced from the velocity vector diagram by remembering that the streamlines are the curves which are everywhere tangent to the velocity. It should be noted that the existence of circulation as in (3) does not imply that particles of fluid actually rotate completely around the body forming closed streamlines. If the circulation is large enough compared to V and the size of the body, such closed streamlines may exist; however, usually combined flows of practical importance do not have closed streamlines, but have the general character shown in the diagram. Figures 1·30 and 1·31*

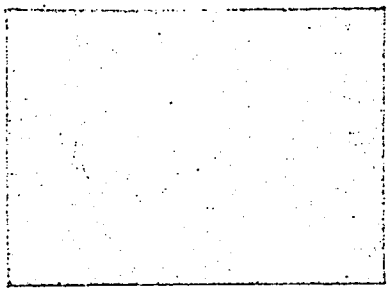

Courtesy of McGraw-Hill Book Co.

FIG. 1·30. Flow around circular cylinder without circulation.

* Reproduced from Prandtl-Tietjens, "Applied Hydro- and Aero-Mechanics," McGraw-Hill Book Co., 1934.

present photographs obtained at Göttingen of flows without and with circulation around a circular cylinder. The streamlines have been made visible and their similarity to those shown diagrammatically in Fig. 1·29 is very striking.

From the results of the earlier discussions a very good estimate of the distribution of velocity and pressure over the surface of the cylinder can be obtained. In the streamline diagrams of Fig. 1·29 the relative magnitudes of velocity and pressure have been indicated by using + to signify "large" and − to signify "small." The only relations used in obtaining the indicated values are those giving the streamline spacing-

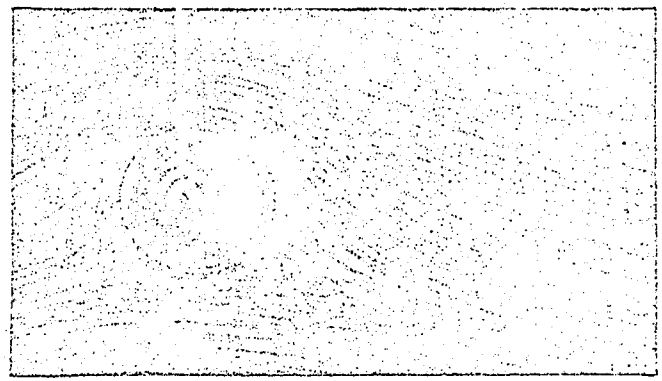

Courtesy of McGraw-Hill Book Co.

FIG. 1·31. Flow around circular cylinder with circulation.

velocity connection, and the Bernoulli theorem. By studying the diagrams with the view of finding the resultant pressure force it can be seen that for the first two flows everything is symmetrical about both a horizontal and a vertical axis through the center of the cylinder. Hence all the pressures balance one another and there is no resultant force. In the third diagram a lack of symmetry appears for the first time, but only about the horizontal axis. The figure is still symmetrical about the vertical axis so that the pressures to the right are balanced by equal pressures to the left on the other side of the symmetry axis. Hence there is no resultant force to left or right, i.e., no drag force. However, the pressures below are high and those above are low so that there is a resultant vertical force which is perpendicular to V and hence appears as a lift as indicated on the diagram.

The results obtained in this very elementary fashion for the especially simple case of a circular cylinder are proved by hydrodynamic theory to have a much wider range of applicability. In fact, for the

teady, two-dimensional flow of a perfect fluid about a cylindrical body
f any shape whatever, the following statements may be rigorously
roved to be correct:*

(*a*) The drag is zero.
(*b*) In the absence of circulation around the body the lift is zero.
(*c*) If there is a circulation of magnitude Γ around the body and if the rectilinear flow velocity past the body is V then a lift exists, the magnitude per unit length perpendicular to the flow being given by

$$L' = \rho V \Gamma \qquad \text{Kutta-Joukowsky law} \qquad [1\cdot18]$$

(*a*) and (*b*) together constitute what is known as D'Alembert's
aradox and were for many years after their discovery in 1744 con-
idered as indicating the uselessness of any theoretical approach to the
ractical problems of fluid mechanics. It is now realized that they rep-
esent a very important first approximation in a wide field of aerody-
amic phenomena. The third statement (*c*) furnishes the foundation for
he entire modern conception of flight. This famous law can be quali-
atively visualized very easily as follows: Consider a body moving
orizontally to the left through a stationary fluid. Then, relative to
he body, the fluid is flowing from left to right. Suppose that the body
as a clockwise circulation when looking in such a direction that the fluid
omes from the left and moves off to the right. Then above the body
he rectilinear flow velocity and the circulation flow velocity are in the
ame direction so that they are added. Below the body the circulation-
ow velocity is in the opposite direction to the rectilinear flow so that the
irculation-flow velocity is subtracted from the rectilinear-flow velocity.
Hence above there is a high velocity and a resulting low pressure
hile below there is a low velocity and hence a high pressure. The
ombination of pressures produces an upward force or lift which is pro-
ortional to the rectilinear velocity and the circulation. This physical
icture was first given by Lord Rayleigh, but the precise mathematical
elationships were worked out in the early 1900's by the German mathe-
atician Kutta and the Russian scientist Joukowsky, whose names have
een attached to the final law, equation 1·18.

Figure 1·32 shows schematically two types of flow around a wing
ection or airfoil at a low and a high angle of attack. The first, (*a*),
epresents flow with zero circulation, while the second, (*b*), corresponds
o the same flow with non-vanishing and specified circulation. The
haracteristic feature of the flow without circulation, (*a*), is that the

* Flows with velocity discontinuities are here not considered.

fluid flows around the pointed trailing edge to the downstream stagnation point on the upper surface. If the trailing edge is sharp, as by definition it is for an airfoil, its radius of curvature is zero and hence, from the concentric circle flow discussion, the velocity around it is infinite. In order to eliminate this infinite velocity Kutta in 1902 assumed that a circulation is set up around the airfoil of strength just sufficient to move the rear stagnation point downstream to the trailing edge. The flow would then stream smoothly off both upper and lower surfaces leaving the airfoil just at the trailing edge and eliminating the infinite velocity. Although Kutta could not give a physical explanation for this phenomenon experiment shows that his assumption accurately

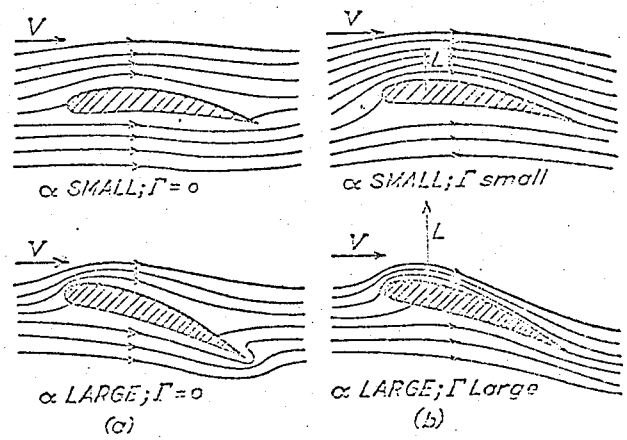

FIG. 1·32. Flows around an airfoil without and with circulation.

corresponds to reality, and some years later Prandtl gave a complete description which will be discussed in section 1–7.

Several important elements of the flow around airfoils can be inferred from the diagrams of Fig. 1·32. Probably the most important is the relation between Γ and the angle of attack α. It is clear that, for the flow without circulation, the rear stagnation point moves further and further from the trailing edge as α increases. Hence the strength of the circulation required to keep the stagnation point at the trailing edge increases with α. Theory and experiment agree in the result that over the range of practically used angles of attack Γ is proportional to α_a, where α_a is called the absolute angle of attack and represents the angle of attack measured from the zero-lift attitude of the airfoil where $\Gamma = 0$.

Since circulation is a sum or integral of terms of the form (velocity × length) it is seen that the dimensions of Γ are $|\text{velocity}| \times |\text{length}|$. The only velocity which appears in Fig. 1·32 is the flow velocity V,

and the most convenient length is the airfoil chord c. Accordingly we write

$$\Gamma \sim Vc\alpha_a$$

or, using $\frac{1}{2}a_0$ to denote the constant of proportionality

$$\Gamma = \tfrac{1}{2}a_0 Vc\alpha_a \qquad [1\cdot19]$$

From equation 1·18 this gives for the lift per unit length of the cylindrical airfoil (perpendicular to the plane of the diagram)

$$L' = a_0\alpha_a \tfrac{1}{2}\rho V^2 c \qquad [1\cdot20]$$

In equation 1·7 we have already given an expression for the total lift on a wing:

$$L = C_L \tfrac{1}{2}\rho V^2 S$$

where S is the wing area. If we use this same form for the lift of unit span of a wing of chord c, then $S = c \times 1$ and we have

$$L' = C_L \tfrac{1}{2}\rho V^2 c \qquad [1\cdot21]$$

Comparing equations 1·20 and 1·21 we obtain

$$C_L = a_0\alpha_a \qquad [1\cdot22]$$

so that the lift coefficient is proportional to the angle of attack (cf. Fig. 1·12). If α_a is measured in radians (1 radian = 57.3°) then hydrodynamic theory gives

$$a_0 = 2\pi \qquad \text{(Theory)} \qquad [1\cdot23]$$

for conventional thin airfoils. For practically all modern airfoil sections experimental results for the normal range of flight Reynolds numbers may be expressed in the form

$$\boxed{a_0 = 2\pi\eta \quad \text{where} \quad \eta \doteq 0.90} \qquad \text{(Experiment)} \qquad [1\cdot24]$$

The correction factor η is usually called the "airfoil efficiency factor."

The second important element which appears from Fig. 1·32 is the pressure distribution over the airfoil surface. If, as is customary, the pressure is measured from the undisturbed static pressure in the rectilinear flow far from the airfoil, then at the stagnation point the pressure will have its maximum value of $q = \frac{1}{2}\rho V^2$, i.e., the full dynamic pressure. Referring to the figure it is seen that over the entire lower surface the pressure will be high, although not as high as q since the fluid is moving, even if relatively slowly. Over the leading edge, particularly on the upper surface, the velocity is higher than V so that the pressure is lower than the reference pressure and we have a suction. Proceeding

downstream along the upper surface the intensity of this suction decreases until at the trailing edge it reaches nearly the undisturbed static pressure again. The intensity of the suction peak near the leading edge increases rapidly as α increases. Figure 1·33 shows typical airfoil pressure distribution diagrams in which all pressures are made dimensionless by dividing by q, pressures greater than the free-stream static pressure are called positive, and pressures lower than this reference

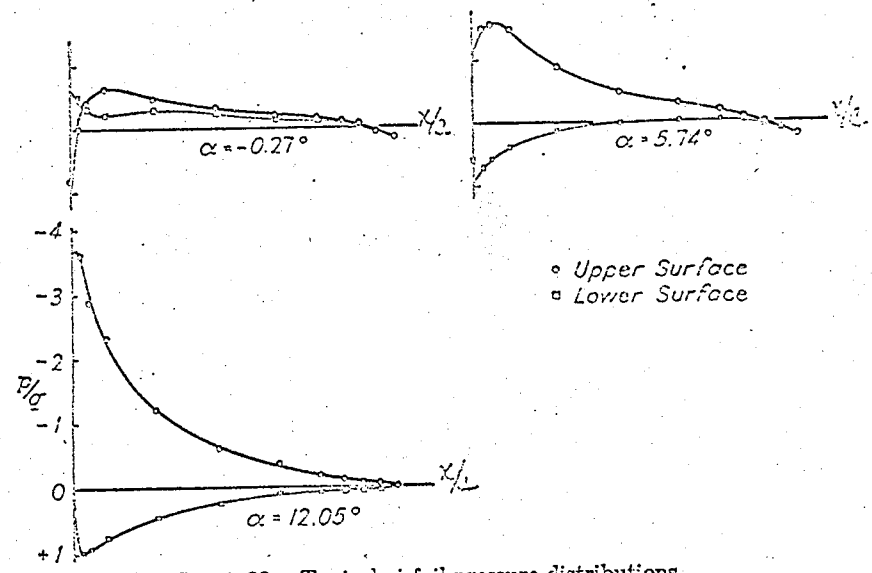

FIG. 1·33. Typical airfoil pressure distributions.
(From *N.A.C.A. Tech. Rep.* 614, Fig. 3.)

pressure are called negative. The lift is approximately proportional to the area inside the curve.

1-6. The Wing of Finite Span; Prandtl Wing Theory

The most important features of the two-dimensional flow of a perfect aerodynamic fluid about cylindrical bodies perpendicular to the flow have now been discussed. These considerations have led to an explanation of lift but not of drag. The latter force component first appears when the discussion is extended to the case of wings of finite span. Here it is obvious that the flow is not identical in all planes perpendicular to the span, so that the generalization really consists in the extension from two- to three-dimensional flow. The most satisfactory treatment of this problem of the three-dimensional flow over a wing of finite span was given by Prandtl in 1918, although the basic ideas were first discussed by

him in 1911, and had been realized still earlier by Lanchester. Prandtl's treatment is intimately connected with certain properties of vortices, which must therefore be stated before the wing problem itself can be treated.

A vortex was defined in connection with two-dimensional motions as the point at the center of a circulation flow where the velocity became infinite. In three dimensions the theorem of the constancy of circulation holds exactly as in two dimensions, i.e., in a flow with circulation the circulation is the same around every path enclosing a given body or vortex. Hence if the length of the path around a vortex is shrunk to zero the velocity becomes infinite at the vortex. The curve connecting the points where this occurs is called a vortex filament. The strength of the vortex at any point along the filament is defined as the magnitude of the circulation around the filament. The vortex laws, which are proved in the hydrodynamic theory of perfect fluids, and which are important here, may be stated as follows:

(*a*) A vortex filament cannot have an end but must either continue to infinity or form a closed path. This is the same property as was found in Section 1–3 in connection with streamlines.
(*b*) The strength of such a vortex filament is constant along its length.
(*c*) Vortices in a fluid always remain attached to the same particles of fluid.

These are called Helmholtz' vortex theorems and were first given by Helmholtz in 1858. A related theorem which we shall require later was given at about the same time by Thomson (Lord Kelvin) and is called Thomson's theorem:

(*d*) The circulation around any path which is always made up of the same fluid particles is independent of the time.

All these theorems are based on the fact that in a perfect fluid no tangential forces can act, and hence the angular velocity of a fluid particle can never change since no couple can be exerted on it. We shall not attempt any further explanation of the theorems but shall proceed with their application to the problem of the finite wing.

Earlier it was seen that in two dimensions the existence of lift was associated with the presence of circulation and it can be shown that the same relation must hold in three dimensions. Accepting this result it follows that around every section of a finite lifting wing there must exist a circulation, Γ. As far as the lift is concerned conditions would be unaltered if the solid wing were replaced by a vortex having the same strength, Γ, since in both cases the lift per unit span is given by the Kutta-Joukowsky law

$$L' = \rho V \Gamma$$

The vortex filament which replaces the wing without altering the lift, is called by Prandtl the lifting line. In order to indicate that the vortex itself has no physical reality in the fluid but is in effect bound to the inside of the wing it is referred to as a "bound vortex" cf. Fig. 1-34).

Prandtl's fundamental conception was to realize that Helmholtz' vortex laws applied to such bound vortices precisely as if they were ordinary vortices having a physical existence in the fluid. Therefore the theorems (*a*) and (*b*) indicate that the bound vortex cannot end at the wing tips where the lift falls to zero. The only possibility is that they continue laterally out of the wing and become actual physical

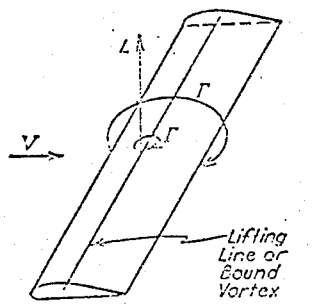

FIG. 1·34. The bound vortex replacing a wing.

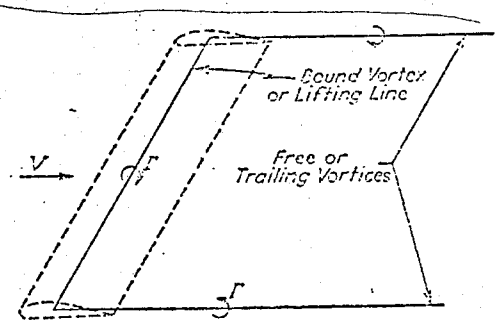

FIG. 1·35. Prandtl's horseshoe vortex system.

vortices in the fluid. In this condition they are called "free vortices" to distinguish them from "bound vortices" which are attached to the wing. Theorem (*c*) requires that these free vortices as they are formed at the wing tips trail off downstream along the streamlines made up of the particles of fluid which strike the tips. They are therefore often referred to as trailing vortices. If the motion is a steady one, the trailing vortices continue downstream to infinity. In order to simplify the picture and make calculations possible Prandtl assumes that the trailing vortices follow the undisturbed streamlines, which are straight lines parallel to V drawn through the wing tips, rather than following the actual streamlines from the tips. This approximation is found to lead to negligible errors in most practically important cases. The simplified picture of the complete system of vortices is now as indicated in Fig. 1·35 and is often called the horseshoe vortex pattern. As appears on

the diagram, the strength of the trailing vortices must be the same as that of the bound vortex and the sense of rotation is from outside — over — in as indicated.

Each of the trailing vortices has associated with it a circulatory motion like that shown in Fig. 1·21 for flow around a cylinder. Hence a view from in front would show a streamline pattern and velocity distribution like those indicated in Fig. 1·36 where the top half of the diagram shows the streamlines in a vertical plane through the lifting line, and the lower half shows the velocity at the wing which is directed vertically downward and is called the "downwash velocity, w." The distribution of w over the span can be estimated from the fact that the velocity associated with each trailing vortex follows the law already deduced for two-dimensional flow (equation 1·14), namely $v \sim \Gamma/r$ where r is the distance from the vortex in question. The downwash

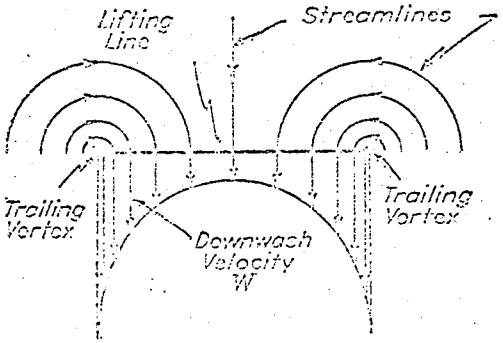

FIG. 1·36. Streamlines and downwash associated with trailing vortices.

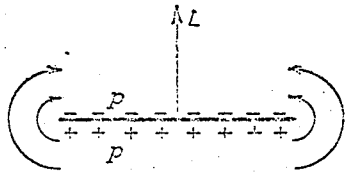

FIG. 1·37. Lateral flow arising from pressure distribution.

velocity w is obtained by adding the velocities associated with the two trailing vortices.

Two justifications for the above picture can be given at this point before proceeding further with the analysis. First, consider the distribution of pressures which must exist above and below a wing which is furnishing lift. The front view of Fig. 1·37 shows the high pressures below (+) and the low pressures above (−) which combine to give the lift. At the tips there must be a lateral flow from the high pressure around to the low pressure. This lateral flow around the tips is that shown in Fig. 1·36 associated with the trailing vortices. Second, the trailing vortices can be made visible by smoke and are sometimes observed in flight, when planes are maneuvering in atmospheric conditions which are such as to make water condensation occur in the reduced-

pressure region of the trailing-vortex cores. These vortices then appear as filaments of mist or fog trailing behind the wing tips.

Returning to the problem, consider the conditions which exist at an airfoil section of the wing lying between the two tips. At this section there exists the rectilinear-flow velocity, V, which, if the span were infinite so that the trailing vortices were infinitely far away, would be the only outside velocity. The flow would then be two-dimensional and the results of the previous section would be applicable. However, because of the finite span there actually exists, in addition to the velocity V, a finite downwash velocity w at the airfoil section, so that the resultant velocity is V_{res} as indicated in Fig. 1·38. Prandtl now assumes that the conditions at the airfoil section are the same as if the latter were a section of a cylindrical wing in a two-dimensional flow with rectilinear velocity V_{res}. In other words, as far as an observer located on the section is concerned he experiences only the rectilinear flow, V_{res}, without knowing whether it actually comes from infinity or not. From this it follows that the lift per unit length of span at the section is given by $\rho V_{res}\Gamma$ and is perpendicular to V_{res}, since the results of the two-dimensional theory are carried over to the present case. This lift is the only force acting on the section and is indicated by the vector R' (representing resultant force per unit length of span) on the diagram. For an observer considering the forces on the wing as a whole the lift will be defined as the component of the resultant force perpendicular to the true velocity at infinity, V, i.e., to the flight path of the wing if the fluid is considered as at rest and the wing as moving through it. Similarly the drag will be the component of force in the direction of V. Hence the resultant force R' furnishes both a lift component L' and a drag component D' as shown in Fig. 1·38. From the figure we see that the velocity and force triangles are similar, so that

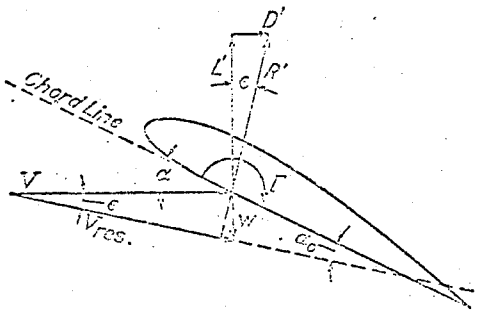

FIG. 1·38. Velocity and force triangles at a wing section.

$$\frac{L'}{R'} = \frac{V}{V_{res}} = \cos\epsilon; \qquad \frac{D'}{L'} = \frac{w}{V} = \tan\epsilon$$

where ϵ is the "downwash angle" between V and V_{res}. It is assumed

in Prandtl's theory and verified by experiment that $w \ll V$, so that ϵ is a small angle and to a first approximation

$$\cos \epsilon = 1; \qquad \tan \epsilon = \sin \epsilon = \epsilon$$

Accordingly

$$L' = R'; \qquad \frac{D'}{L'} = \frac{w}{V} \qquad [1\cdot25]$$

Consideration of the angle of attack shows that the apparent angle of attack of the section (sometimes called the geometrical angle of attack) is the angle between the chord line and the velocity at infinity V. This appears in Fig. 1·38 as α, which is the usual designation. However, to the observer on the airfoil section the angle of attack, which is the angle actually determining the circulation, is that between the chord line and V_{res}. This is shown as α_0 on the diagram and is usually called the "effective angle of attack." In other words the airfoil section at the apparent angle of attack α experiences exactly the same forces as if it were a section of an infinite span wing at an angle of attack α_0 in a two-dimensional flow.

These results may be summarized as follows: The effect of finite span is to introduce trailing vortices which produce a downwash at the wing. This downwash rotates the effective velocity vector which decreases the effective angle of attack and rotates the resultant force vector backwards, so that a drag component is introduced. These two effects are connected with the downwash velocity by the relations:

$$\alpha_0 = \alpha - \frac{w}{V}; \qquad \frac{D_i'}{L'} = \frac{w}{V} \qquad [1\cdot26]$$

The subscript $()_i$ has been attached to the drag symbol because of the fact that this drag force is usually called "induced drag." The downwash velocity w is also often referred to as "induced velocity." The reason for this terminology is that the relation between downwash velocity and trailing vorticity is analogous to that between a magnetic field strength ($\sim w$) and the electric current in a wire ($\sim \Gamma$) inducing the field. The numerical computations involved in Prandtl's theory are identical with calculations developed long ago in the theory of electromagnetic induction, so that the adjective "induced" has been taken from the electrical field and introduced into aerodynamics. It should be pointed out and emphasized that induced drag is not a resistance associated with friction since a perfect, frictionless fluid has been considered throughout. The energy which must be supplied to overcome this drag in the case of a moving airplane is not therefore immediately

dissipated in the form of heat, but is left behind in the fluid as the kinetic energy associated with the circulatory motion around the trailing vortices.

The discussion up to this point has related to conditions at a particular airfoil section of a finite wing. In order to determine the characteristics of the wing as a whole it is necessary to carry out a summation or integration of these elementary effects over the entire span, but difficulties present themselves immediately. For, referring to Fig. 1·36, consider an element very close to one wing tip. Here, since the induced velocity is inversely proportional to the distance from the trailing vortex, $w \to \infty$ as the tip is approached. But a fundamental assumption of the theory was that w is very small. The complete resolution of this contradiction was only achieved by Prandtl's group after years of effort, although it now seems very simple. Instead of considering a single lifting line with its associated trailing vortices, let us visualize a number

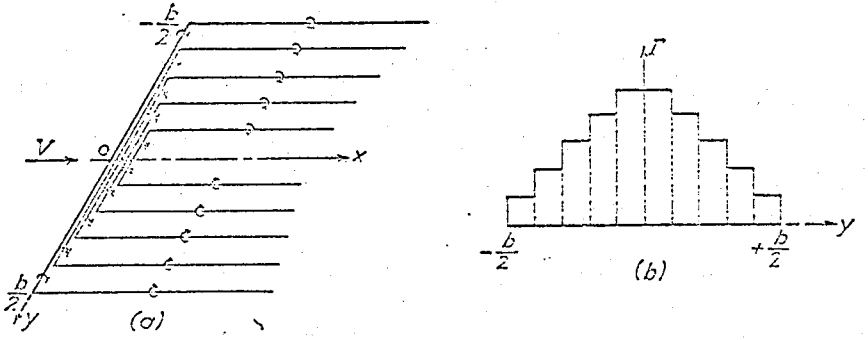

FIG. 1·39. Superposition of finite strength horseshoe vortices.

of such lifting lines of different lengths superimposed on one another as indicated in Fig. 1·39 (*a*) where the x axis is an axis of symmetry parallel to V and the y axis lies along the span. The distribution of trailing vortices appears in (*a*) and the distribution of circulation along the span in (*b*). The distribution of circulation follows from the fact that circulations may be superimposed and the effects added algebraically. Since for every section along the span the Kutta-Joukowsky equation, $L' = \rho V \Gamma$, holds the distribution of lift along the span is exactly proportional to the distribution of Γ. The superposition principle can obviously be carried to the limit in which an infinite number of horseshoe vortices each of infinitesimal strength is added together in the manner suggested by Fig. 1·39. The result indicated in Fig. 1·40 will be a trailing vortex sheet rather than a number of discreet vortices, and a continuous distribution of circulation (and hence of lift) over the span

instead of a stepwise distribution. No single vortex will have a finite strength so that there are no infinite values of the downwash, and the difficulties mentioned above disappear.

With this very flexible picture it is possible to determine a distribution of the elementary horseshoe vortices which corresponds to any desired lift distribution over the span. The distribution of circulation or bound vorticity determines that of the trailing vortices and hence of the downwash velocity, so that the lift and downwash distributions are very closely related. The downwash in turn determines the effective angle of attack in accordance with equation 1·26 and this, in connection with the airfoil section geometry, specifies the circulation at any point of the span. The working out of this complex set of interrelationships to give the characteristics of a given wing involves very lengthy and elaborate calculations which will later be discussed briefly.

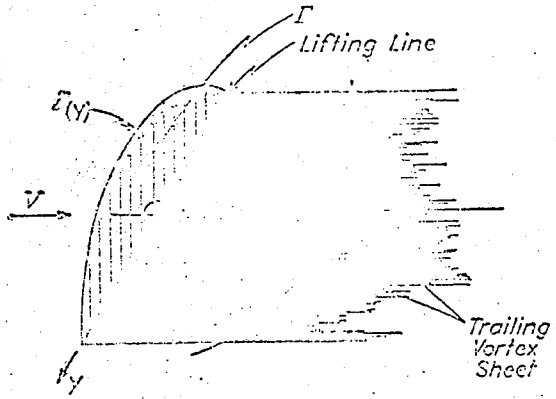

FIG. 1·40. Continuous distribution of circulation and trailing vorticity.

However, there is one particular type of lift distribution, discovered by Prandtl, for which everything is very simple. This is the so-called "elliptic lift distribution." If y represents distance along the span from the center of the wing (cf. Fig. 1·39), b the wing span, L' the lift per unit length along the span at an arbitrary point y, and L'_0 the value of L' at the center of the wing, then the elliptic lift distribution is expressed analytically by

$$L' = L'_0\sqrt{1-\left(\frac{y}{b/2}\right)^2} \qquad [1\cdot27]$$

or

$$\frac{L'^2}{L'^2_0}+\frac{y^2}{(b/2)^2}=1$$

The reason for the name is apparent since a plot of L' vs. y has the shape of an ellipse.

The special properties associated with the elliptic lift distribution are

(*a*) The downwash is constant along the span.

(*b*) For a given total lift, span, and velocity V the induced drag has its lowest possible value.

(*c*) The elliptic distribution theoretically occurs for an untwisted wing of elliptical plan form.

(*d*) Lift distributions over untwisted wings of conventional tapered plan forms are theoretically and experimentally found to approximate closely to the elliptical shape.

The simplifications accompanying these special properties are so great that practically all preliminary calculations for normal wings are based on the assumption of this optimum elliptical lift distribution. In particular the property (*a*) implies that the velocity triangle of Fig. 1·38 is identical for every airfoil section along the span. In other words the ratio $D'_i/L' = w/V$ (equation 1·26) has the same value at every wing element. When the forces on all these elements are added together to furnish the total wing force, it follows that the total induced drag and lift have the same relation, i.e.,

$$\frac{D_i}{L}=\frac{w}{V}$$

or dividing numerator and denominator of the left side by $\frac{1}{2}\rho V^2 S$ to give force coefficients

$$\frac{C_{D_i}}{C_L}=\frac{w}{V}$$

If the "induction" calculations are carried out for this case of elliptical lift distribution a very simple result is obtained for the downwash. This result is so basic to most aerodynamic calculations that it belongs with the Bernoulli theorem and the Kutta-Joukowsky law in the category of the few formulas which the aerodynamicist must memorize. It is

$$\frac{w}{V}=\frac{C_L}{\pi AR}$$

where

$$AR = \text{Aspect ratio} = \frac{b^2}{S}$$

For a wing with rectangular plan form the aspect ratio is simply the ratio of span to chord.

Collecting the above results we obtain the primary relations given by the simple Prandtl wing theory:

$$\left.\begin{aligned} &\frac{w}{V} = \frac{C_L}{\pi AR} = \text{Constant over the span} \\ &\alpha_0 = \alpha - \frac{C_L}{\pi AR} \\ &C_{D_i} = \frac{C_L^2}{\pi AR} \end{aligned}\right\} \quad \begin{matrix}\text{Elliptic} \\ \text{lift} \\ \text{distribution}\end{matrix} \qquad [1\cdot28]$$

An alternative form of the last relation which is very convenient for many purposes is obtained by multiplying both sides of the equation by qS where q is the dynamic pressure $\frac{1}{2}\rho V^2$:

$$C_{D_i}qS = \frac{C_L^2 qS}{\pi AR} \cdot \frac{qS}{qS} = \frac{(C_L qS)^2}{\pi(b^2/S)qS} = \frac{L^2}{\pi q b^2}$$

Therefore

$$D_i = \frac{L^2}{\pi q b^2} \qquad [1\cdot29]$$

This form is especially useful when calculations of total force are desired. In equations 1·28 and 1·29 the quantities C_L, C_{D_i}, L, and D_i refer to

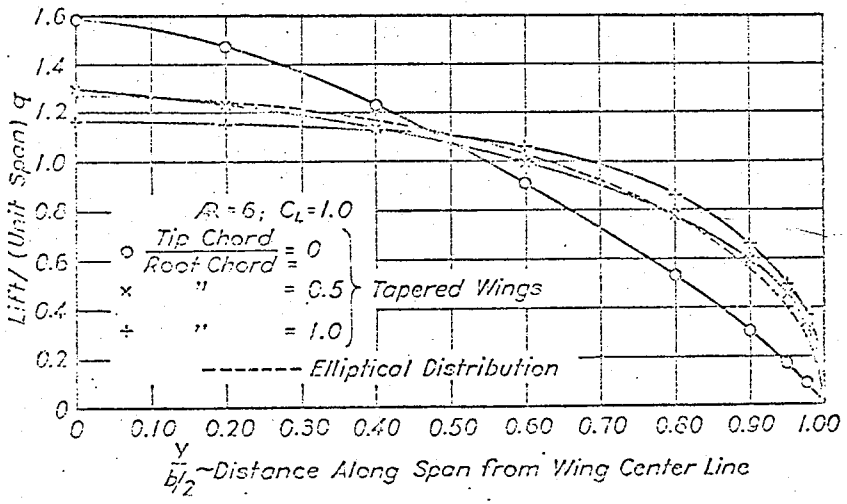

Fig. 1·41. Lift distributions over elliptical and tapered wings.

the over-all characteristics of the wing rather than to the characteristics of any particular section along the span.

Figure 1·41 presents the results of calculations giving the distribution of lift over the semi-span of several untwisted wings of aspect ratio 6, having taper ratios covering the range of values normally employed on contemporary airplanes. The curves are plotted from tabular data pre-

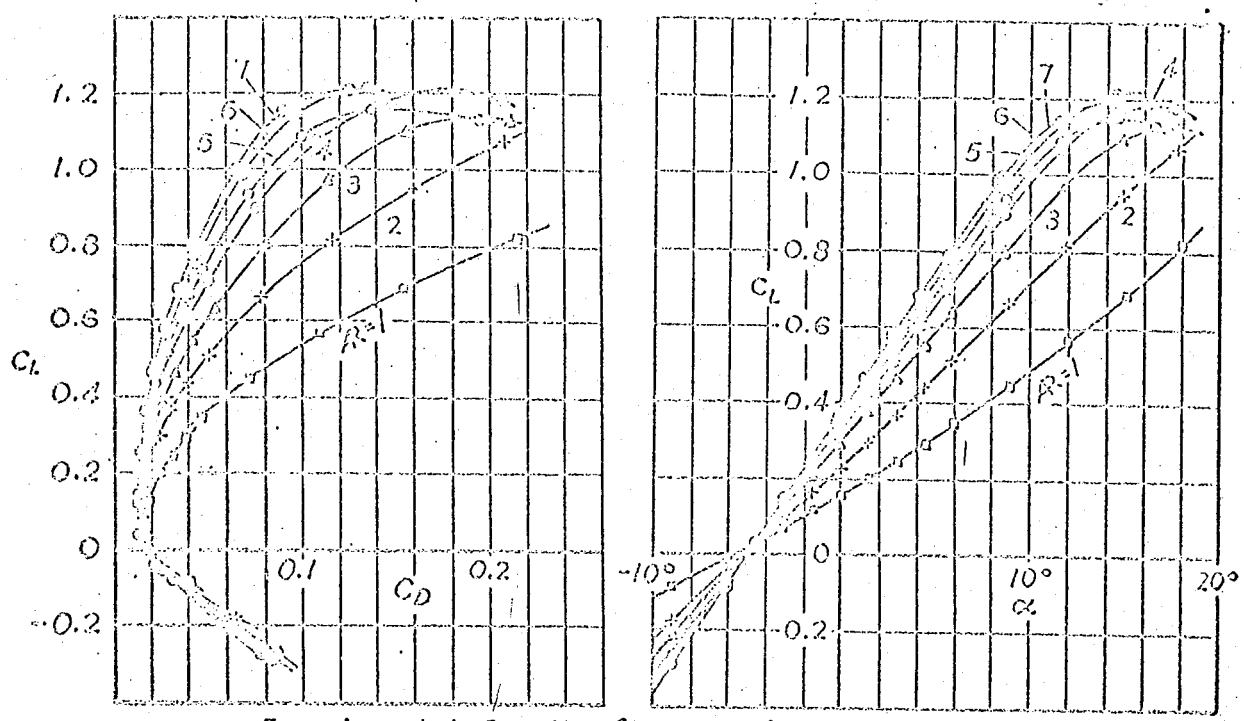

Experimental Results for a Series of Wings of Different Aspect Ratios

Experimental Results Corrected to Aspect Ratio 5

Fig. 1·42. Experimental verification of Prandtl wing theory.
(From *N.A.C.A. Tech. Rep.* 116.)

sented by Anderson.* The elliptical lift distribution is also i[illegible] for comparison, and the various lift distributions are seen to approximate fairly closely to the elliptical shape, in agreement with property (*d*) mentioned above following equation (1·27).

Before discussing the further extensions of the theory to cases involving other lift distributions it will be desirable to consider some of the consequences of the results obtained thus far. Probably the most important is that giving the dependence of total wing drag on plan form or, more precisely, on aspect ratio. The fundamental assumption in this connection is that the induced drag of a wing represents that portion of the total drag which depends on wing plan form, any remaining drag depending on the shape of the airfoil profiles which make up the wing. This assumption implies that if two untwisted rectangular wings, 1 and 2, having the same airfoil section and chord, but differing in span or aspect ratio, are tested under similar conditions their drag coefficients will differ only by the amount of the difference in induced drag coefficients:

$$C_{D_1} - C_{D_2} = \frac{C_L^2}{\pi AR_1} - \frac{C_L^2}{\pi AR_2} = \frac{C_L^2}{\pi}\left(\frac{1}{AR_1} - \frac{1}{AR_2}\right) \qquad [1\cdot30]$$

Similarly the apparent angles of attack at which the two wings will attain a given value of C_L will differ by the downwash angle difference for the two wings:

$$\alpha_1 - \alpha_2 = \frac{C_L}{\pi}\left(\frac{1}{AR_1} - \frac{1}{AR_2}\right) \qquad [1\cdot31]$$

The relations given by equations 1·30 and 1·31 furnish a very powerful tool whereby tests need be made at only one aspect ratio, the characteristics for any other aspect ratio being obtained by simple calculations from those at the original one. These relations also permit a relatively easy but powerful experimental check to be made of the theory. Such a check was carried out at Göttingen under Prandtl's direction soon after the theory was developed. A series of wings identical in all respects except aspect ratio was tested in the wind tunnel. The results, shown in Fig. 1·42, exhibit first the great differences in wing characteristics for the various aspect ratios, and second the remarkable agreement when all of the results are converted to an aspect ratio of 5 using equations 1·30 and 1·31. When it is remembered that the theory is based on the replacement of a wing by a lifting line with zero chord, the fact that the predictions of the theory are accurately substantiated by experiment for aspect ratios as small as 2 is very astonishing.

* Raymond F. Anderson, "Determination of the Characteristics of Tapered Wings," *N.A.C.A. Tech. Rep.* 572 (1936).

Equations 1·30 and 1·31 assume an especially useful form if the second of the two wings to be compared is taken as having infinite aspect ratio. The subscript $()_0$ is applied to the C_D and α for this wing to indicate that the corresponding aspect ratio is infinite. Then dropping the subscript $()_1$

$$\left.\begin{aligned} C_D &= C_{D_0} + \frac{C_L^2}{\pi AR} \\ \alpha &= \alpha_0 + \frac{C_L}{\pi AR} \end{aligned}\right\} \qquad [1\cdot32]$$

The drag coefficient C_{D_0} corresponding to infinite aspect ratio is called the "profile drag coefficient." The angle of attack α_0 for the same case has already been discussed as the effective angle of attack. Both α_0 and C_{D_0} depend only on airfoil profile shape and are independent of wing plan form. In the past it was often customary to present airfoil characteristics corresponding to some standard aspect ratio (usually 5 or 6) and then to convert these data to any particular aspect ratio desired using equations 1·30 and 1·31. In recent times the much simpler procedure has been widely adopted of presenting infinite aspect ratio characteristics $C_{D_0}(C_L)$ and $\alpha_0(C_L)$ and converting these directly to any aspect ratio using equations 1·32.

It will be noticed that in the preceding sentence $\alpha_0(C_L)$ was written rather than $C_L(\alpha_0)$. This was done in order to emphasize the fact that the fundamental variable in the majority of problems involving wings is most conveniently taken as C_L. One is likely to think of the geometrical variable, angle of attack, as the independent variable and all others as dependent. However the fundamental position of C_L in the Prandtl theory makes it much more satisfactory to give this variable the basic role and to consider the others as depending on it. In other words, it is preferable to think in terms of setting a C_L and finding to what angle of attack the wing must be rotated, rather than in terms of setting an α and calculating the C_L to be expected. We shall see later that this is even more applicable when we consider the actual flight of an airplane.

One result of the Prandtl induction theory which has not yet been considered and which will be stated without proof is: "The relation between pitching moment coefficient C_M and C_L is independent of the aspect ratio." It is obvious that this is not true of the relation between C_M and α. This fact furnishes an additional reason for the choice of C_L rather than α as the independent variable.

Figure 1·43 presents typical infinite aspect ratio results for a conventional airfoil section, presented in a form which has been widely

adopted. The symbol $C_{M_{0.25}}$ means that the moment coefficients presented are referred to a moment axis located on the chord line 25 per cent of the chord length aft of the leading edge. If we consider only the

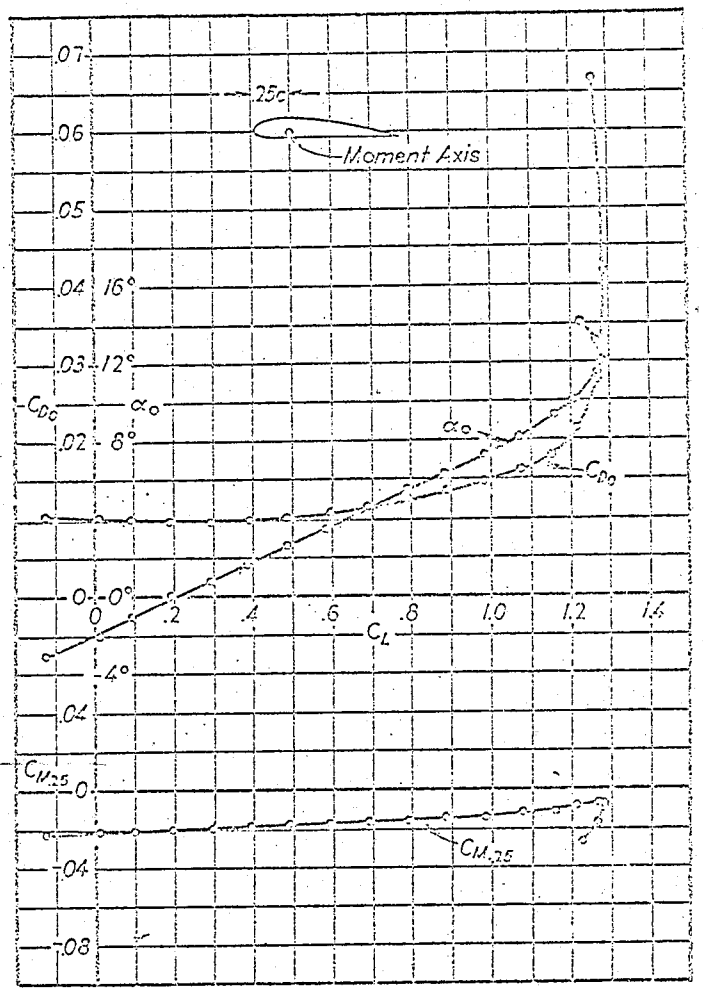

FIG. 1·43. Typical infinite aspect ratio wing characteristics.
(From *tests at the GALCIT*; R = 1,200,000.)

region between zero lift and $C_L = 1.0$, which corresponds to the normal flying range, we see that the curves exhibit certain very simple characteristics:

(*a*) The C_L vs. α_0 curve is practically a straight line.
(*b*) The C_M vs. C_L curve is also practically a straight line.

(c) C_{D_0} is very roughly constant. (This is much less accurate than a or b.)

These characteristics will be taken up in more detail in the section on *Airfoil Characteristics*. Here it is necessary only to point out that the linear relation between C_L and α_0 has already been discussed in section 1·5 where the symbol a_0 was chosen for the slope of the C_L vs. α_0 curve.

If the typical infinite aspect ratio characteristics (a) and (c) above are introduced into equations 1·32, it is possible to draw certain conclusions regarding the characteristics of wings with finite aspect ratio.

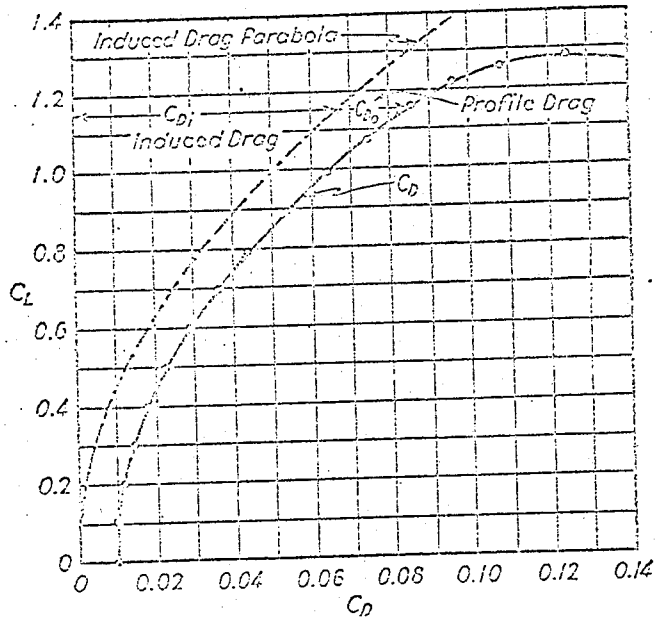

FIG. 1·44. Polar diagram for a wing.

Considering first the drag coefficient, it appears that a wing polar (Fig. 1·44), as the plot of C_L vs. C_D is called, has approximately the shape of a parabola for $0 < C_L < 1$. This first approximation of a parabolic polar will be the starting point for much of the later performance analysis.

Turning now to the angle of attack, it is convenient to introduce the notation $\alpha_{L_0} = \alpha$ for $C_L = 0$

$$\alpha_e = \alpha - \alpha_{L_0} \qquad [1\cdot33]$$

Note that, in accordance with equations 1·32, at $C_L = 0$ the geometrical and effective angle of attack are equal, $\alpha = \alpha_0$, so that α_{L_0} refers equally to α and α_0. Now we have seen that theory and experiment agree in

giving a linear relation between C_L and α_0, the constant of proportionality having been written as a_0, so that

$$C_L = a_0(\alpha_0 - \alpha_{L_0}) \qquad [1\cdot34]$$

In view of the linear relation between α, α_0, and C_L given by equation 1·32 a similar relation would be expected to hold between C_L and α. If the constant of proportionality in this case is written as "a" the anticipated relation would have the form

$$C_L = a(\alpha - \alpha_{L_0}) \qquad [1\cdot35]$$

It is now necessary to verify this relation and at the same time find the connection between a and a_0. By subtracting α_{L_0} from both sides of the second equation of 1·32

$$\alpha - \alpha_{L_0} = (\alpha_0 - \alpha_{L_0}) + \frac{C_L}{\pi AR}$$

From equation 1·34

$$(\alpha_0 - \alpha_{L_0}) = \frac{C_L}{a_0}$$

and substituting this in the equation just above

$$\alpha - \alpha_{L_0} = \frac{C_L}{a_0} + \frac{C_L}{\pi AR} = \frac{C_L}{a_0}\left(1 + \frac{a_0}{\pi AR}\right)$$

Hence

$$C_L = \frac{a_0}{1 + \dfrac{a_0}{\pi AR}}(\alpha - \alpha_{L_0})$$

which is exactly of the form of equation 1·35 if

$$a = \frac{a_0}{1 + \dfrac{a_0}{\pi AR}} \qquad [1\cdot36]$$

The simple Prandtl theory for the case of elliptical lift distribution therefore gives a definite relation between the "lift curve slopes" for infinite and finite aspect ratio. The relation in equation 1·36 will appear later very importantly in the *Airplane Stability* analysis.

It only remains in concluding this section to outline the modifications to the above results which are introduced when the lift distribution is not elliptical. Although the theoretical calculations are much more complicated in this case because of the fact that the downwash is no longer constant across the span, the final results for untwisted wings appear in a

quite simple form. It is only necessary to modify equations 1·32 as follows:

$$\left.\begin{aligned} C_D &= C_{D_0} + \frac{C_L^2}{\pi R}(1+\delta) \\ \alpha &= \alpha_0 + \frac{C_L}{\pi R}(1+\tau) \end{aligned}\right\} \quad \text{Non-elliptic lift distribution} \qquad [1\cdot37]$$

where δ and τ are small correction factors depending on the deviation of the lift distribution from the ideal elliptical form. Figure 1·45 shows values of the induction factors δ and τ as calculated by Glauert for

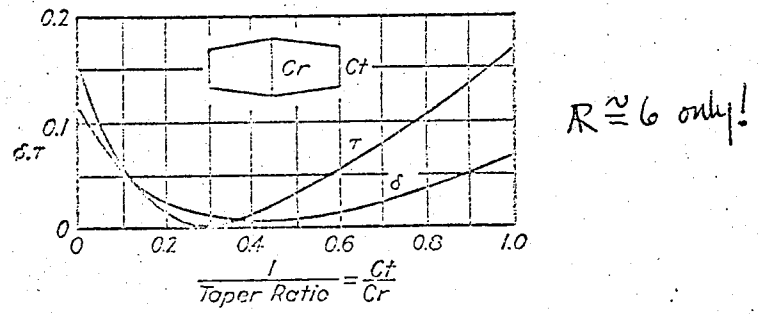

R ≅ 6 only!

FIG. 1·45. Induction factors for non-elliptic lift distribution.

straight-tapered, untwisted wings of aspect ratio about 6. It appears that for normal taper ratios, C_r/C_t, the correction for induced drag is so small as to be negligible, while that for angle of attack may become large enough to require consideration for nearly rectangular wings ($C_t/C_r \doteq 1$).

1–7. Effects of Viscosity at Large Reynolds Numbers; The Boundary Layer

All the theoretical considerations thus far have been based on the assumption of perfect fluids, i.e., viscosity has been entirely neglected. Even with this extreme over-simplification the theory has explained a group of phenomena of tremendous importance. The lift of airplane wings and the associated induced drag have not only been physically clarified, but quantitative predictions agreeing remarkably well with experiment have even been made possible. Three types of phenomena have, however, already been encountered which the theory has been helpless to elucidate. These are

(*a*) The deviation of the flow pattern from that predicted at the rear of bluff bodies like circular cylinders.

(*b*) The limitation to the values of C_L which can be attained with airfoils, and the deviations from the predicted airfoil characteristics in the maximum lift region (cf. Fig. 1·12, 1·43).

(*c*) The existence of profile drag (cf. Fig. 1·44).

The physical mechanism by which circulation develops around a wing is also not yet clear. All of these points represent failures of the theory, associated with its basic assumption of perfect fluids, and all are satisfactorily explained by the famous boundary layer theory introduced by Prandtl in 1904 to describe the influence of viscosity under large Reynolds number flow conditions.

The starting point of Prandtl's considerations is the empirically justified "condition of no slip." This states that whenever a real fluid, no matter how small its viscosity, flows over a solid surface, however smooth, the layer of fluid immediately adjacent to the surface sticks to the surface without any slip whatever.* All of our perfect fluid con-

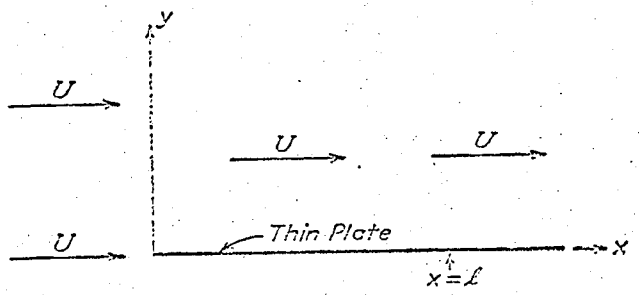

FIG. 1·46. Notation for flow along a flat plate.

siderations have been based on the assumption of zero shearing stress so that the theoretical flows, heretofore considered, slide over solid surfaces without any retardation. In order to investigate the implications of the no-slip condition consider a two-dimensional, steady flow, with uniform velocity and hence constant static pressure, over the surface of a smooth plate set parallel to the flow. A coordinate system attached to the plate is chosen as shown in Fig. 1·46, and the undisturbed velocity far from the plate is denoted by U. The plate is taken as infinitely thin so that in the case of perfect fluid flow it coincides with one of the undisturbed streamlines and produces no disturbance whatever, since the fluid adjacent to the surface slips over the latter with the velocity U.

* The only exception to this statement which has been found experimentally occurs in highly rarefied gases when the mean free path of the molecules becomes large compared to the dimensions of the solid body in question. Such cases never occur in practical aeronautical problems.

Figure 1·47 contains on the left the velocity profile at some point $x = l$ for this perfect fluid flow. On the right are drawn a corresponding series of profiles for real fluids with different values of μ. All the profiles on the right have the common features that

(*a*) far from the surface ($y \to \infty$) the local velocity $u = U$, and
(*b*) at the surface ($y = 0$) $u = 0$.

If the viscosity is small it is physically apparent that the disturbing effect of the plate will extend only a relatively short distance from the plate, while if the viscosity is large the layers of fluid much further away

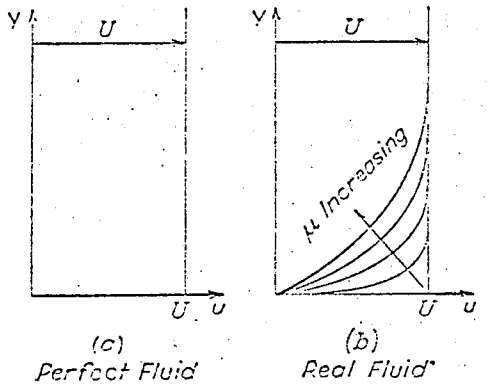

FIG. 1·47. Velocity profiles for the flow of Fig. 1·46.

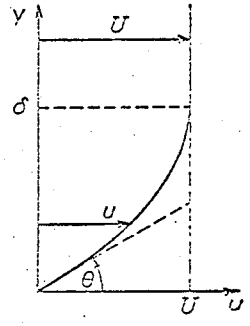

FIG. 1·48. Boundary layer notation.

will be slowed down by the dragging action of the plate. We denote the distance from the wall at which the dragging effect of the plate has become negligible by δ (cf. Fig. 1·48), so that

$$u \doteq U \text{ at } y = \delta \qquad [1\cdot38]$$

Prandtl's boundary layer assumption may be very crudely stated as follows: "When a fluid has very small viscosity, $\mu \to 0$, the thickness of the fluid layer affected by viscosity is very small, $\delta \to 0$. This layer, $0 \leq y \leq \delta$, is called the boundary layer." The statement in this form, although it represents the essential elements of the theory, is actually meaningless since "small" is not compared to anything. A more correct, if less transparent, statement is the following: "If l represents distance downstream along the surface from the leading edge of a body in a flow with undisturbed velocity U, and δ is the boundary layer thickness at the point l, then if $R_l = Ul/\nu \gg 1$ then $\delta/l \ll 1$." In this form the comparisons have been given a precise meaning since they are

made in the form of statements that dimensionless ratios have values very large or very small compared to 1. Prandtl's analysis applied to the flat plate flow of Fig. 1·46 actually leads to the result that

$$\frac{\delta}{l} \sim \frac{1}{\sqrt{R_l}} \quad \text{where} \quad R_l = \frac{Ul}{\nu} \qquad [1\cdot39]$$

Equation 1·39 leads to the conclusion that if R becomes very large δ/l becomes very small, so that the flow over the plate with its very thin boundary layer becomes practically identical to that given by a perfect fluid analysis. Let us investigate the behavior of the skin friction under these conditions. For this purpose consider Fig. 1·47(*b*) using the notation given in Fig. 1·48. As $\mu \to 0$ the velocity profile near the wall becomes fuller and fuller so that because of the no-slip condition the slope of the profile at the wall, $\tan\theta$, becomes smaller and smaller and also approaches zero. It was seen earlier in connection with Fig. 1·3 that the velocity gradient $du/dy = 1/\tan\theta$. Hence as $\mu \to 0$, $(du/dy)_0 \to \infty$. Here the subscript $()_0$ denotes conditions at the surface $y = 0$. From equation 1·2

$$\tau_0 = \mu \left(\frac{du}{dy}\right)_0$$

which in the limit $\mu \to 0$ becomes

$$\tau_0 = 0 \cdot \infty$$

This is an indeterminate form which is shown by Prandtl to be proportional to $1/\sqrt{R_l}$. Hence even though R_l becomes very large, a finite skin friction remains which does not vanish until $R_l = \infty$, corresponding to a true perfect fluid. Hence for real fluids with very small viscosity, i.e., flows with very large Reynolds number, the general flow pattern closely approaches that of a perfect fluid, but the shearing stress at the wall remains finite as long as the viscosity does not actually vanish. This finite value of shearing stress means that even at enormous Reynolds numbers there is a definite skin friction and hence a drag force.

The results outlined above can often be carried over with only minor modifications to the case of flow around a body with curved surfaces such as an airfoil or fuselage. An explanation of phenomenon (*c*) of the first paragraph of this section has thus been furnished. For it now appears that for large Reynolds numbers the effect of viscosity may be such as to leave the main perfect fluid flow unaltered so that the airfoil characteristics already deduced are practically unaffected, while a finite skin friction is introduced. This skin friction is, in fact, the profile drag which was completely unexplained by the earlier perfect fluid theory.

We shall return to a more detailed discussion of skin friction in a later chapter and proceed here with more general considerations.

The explanation of phenomena (*a*) and (*b*) rests upon a different aspect of the boundary layer picture. Consider the boundary layer along the surface of a circular cylinder in a rectilinear flow where the conditions are like those shown in Fig. 1·29 (1). Selected boundary layer profiles for this case are shown in Fig. 1·49 with the y coordinate scale enormously expanded. In this figure the coordinate system is curvilinear, the x axis lying along the surface of the cylinder and the y coordinate being perpendicular to it. U represents the velocity in the perfect fluid flow outside the boundary layer at any point x along the surface, and U_0 is the free-stream velocity far from the cylinder.

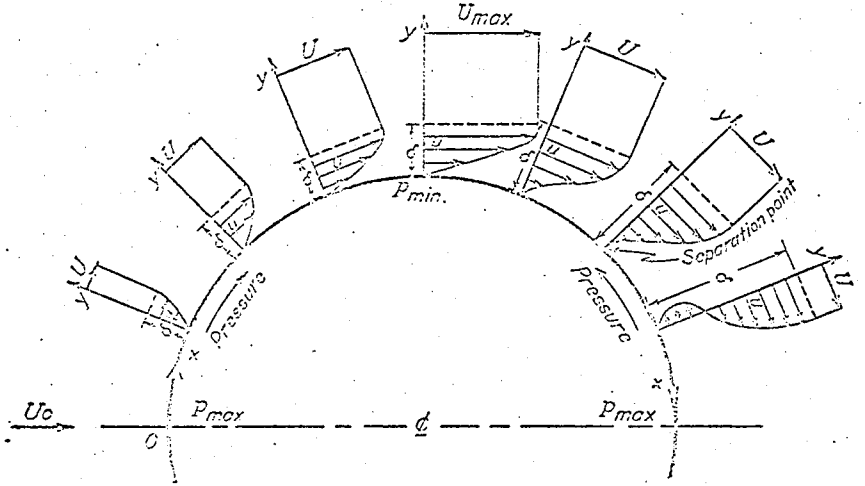

FIG. 1·49. Boundary layer along a circular cylinder.

In accordance with the discussion in section 1–3, U increases from zero at the forward stagnation point, $x = 0$, to its maximum value at the top of the cylinder, and then decreases again as one goes downstream along the rear face. Using Bernoulli's theorem it follows that the pressure first decreases in going downstream from $x = 0$ and then increases again. It is one of the important conclusions of the boundary layer theory that the pressure does not change in going perpendicularly to the flow across the thin boundary layer, so that the pressure across any boundary layer cross section is constant and equal to the value computed by the Bernoulli theorem just outside the boundary layer where viscosity has no effect and the theorem may be applied.

The characteristics of the boundary layer are quite different in the regions of decreasing pressure on the front face and of increasing pressure on the rear face, i.e., the regions of accelerated and decelerated flow. In the first region the velocity profiles are very similar to those which occur in the flat plate flow (cf. Fig. 1·48). The only difference is that now there is a pressure gradient which tends to accelerate all the fluid particles so that the velocity near the wall will be a little higher than if there were no pressure gradient. In other words the boundary layer will be somewhat thinner and the profile a little fuller in the region of accelerated flow than in the case of uniform flow. As soon as the minimum pressure point is passed in the downstream direction, however, conditions become quite different. From this point on the pressure gradient gives a force opposing the velocity so that the fluid particles in the boundary layer are decelerated instead of accelerated. This is, of course, also true of the fluid just outside of the boundary layer. For this outer portion of the fluid the kinetic energy which has been attained at the minimum pressure point, $\frac{1}{2}\rho U_{max}^2$, is just sufficient to carry the fluid against the pressure gradient around to the rear stagnation point before the velocity drops to zero. However, in the boundary layer at the minimum pressure point the kinetic energy is less than $\frac{1}{2}\rho U_{max}^2$ since friction has been retarding the flow and consuming kinetic energy which appears as heat through the action of viscosity. Hence the pressure gradient will slow these particles down and bring them to rest before the rear stagnation point is reached. This will obviously occur first next to the wall where the velocity was lowest at the minimum pressure point. Accordingly in the region of decelerating flow the effect of the pressure gradient is to increase the boundary layer thickness and fundamentally alter its shape by greatly slowing down the velocity near the wall. As is indicated in Fig. 1·49 a "separation point" is eventually reached where the velocity profile has a vertical tangent at the wall and where the fluid particles a little distance out have been brought to rest. Immediately downstream from this point these layers of fluid will obviously be driven backwards, or upstream, by the pressure gradient. Hence a reverse flow occurs near the surface and the main flow leaves or separates from the surface at the separation point as is indicated by the streamline pattern of Fig. 1·50. It is apparent that

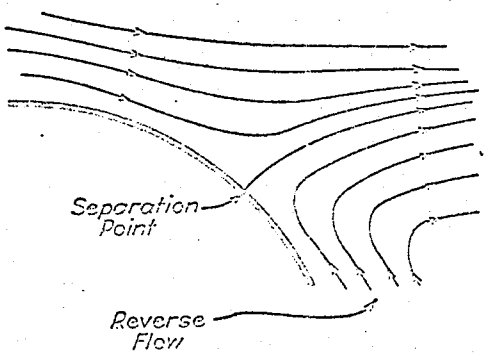

FIG. 1·50. Flow in the neighborhood of a separation point.

downstream from such a separation point the main flow has an entirely different character than that which would be expected from the earlier perfect fluid considerations. Figure 1·51 shows schematically the general characteristics of the flow around a circular cylinder where the

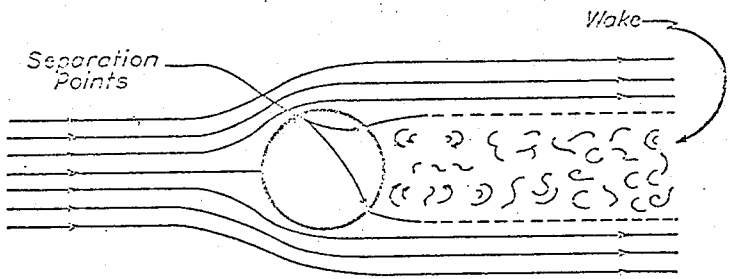

FIG. 1·51. Wake behind a cylinder with separation.

separation points occur shortly behind the minimum pressure points. The reverse flow behind the separation points is very unstable and breaks up into a large number of eddies. At moderate Reynolds numbers these eddies are arranged in a definite pattern known as the Kármán vortex street, an example of which is shown in Fig. 1·52.* At higher Reynolds

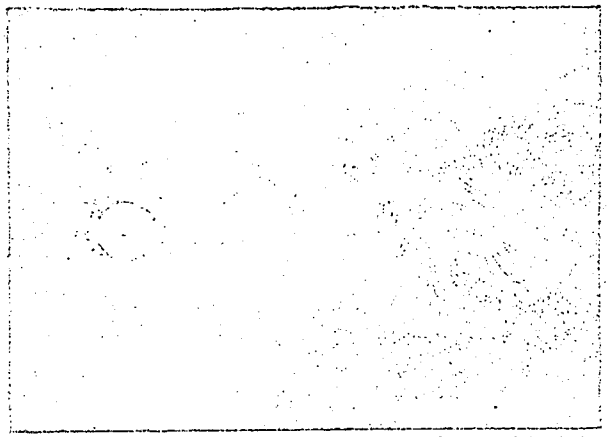

Courtesy of McGraw-Hill Book Co.

FIG. 1·52. Kármán vortex street behind a circular cylinder.

numbers (above, say, 100,000) the flow is completely irregular and eddying or turbulent. In either case the region occupied by the eddying motion is called the "wake." The existence of such a wake means that the main flow streamlines fail to close in behind the body so that

* Reproduced from Prandtl-Tietjens, *loc. cit.*

the stagnation pressure is not developed over the rear surface. This destroys the fore and aft symmetry of the flow pattern and hence of the pressure distribution so that a large pressure drag occurs.

It is now possible to distinguish between streamline and bluff bodies. The former are bodies which are so shaped that the pressure increase downstream from the minimum pressure point is so gradual that separation does not occur at least before the rear of the body is practically reached. The boundary layer is then everywhere extremely thin and the flow and pressure distribution are nearly identical with those which would be expected in the case of a perfect fluid flow. The drag of such bodies is very small, arising almost entirely from skin friction. With bluff bodies, on the other hand, the pressure rise is rapid enough so that separation occurs well ahead of the rear of the body, with the resulting formation of a wake which seriously alters the perfect fluid flow pattern and leads to a pressure drag. Such bodies always have a high drag of which the skin friction is only a small part.

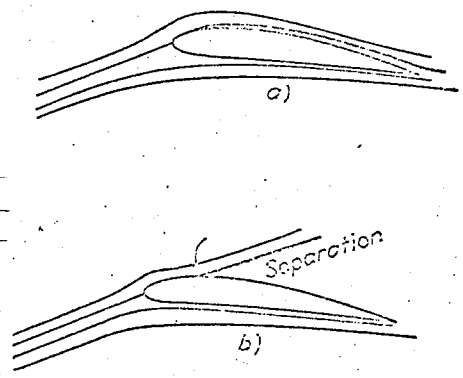

FIG. 1·53. Alternative flows about an airfoil near the stall.

An explanation of phenomenon (*a*) of the first paragraph has thus been given. That for (*b*) is very similar and rests upon the fact that a given body may fall into the "streamline" category at one attitude and into the "bluff" category at another. This is the case for airfoils which at low and moderate angles of attack behave like streamline bodies (Fig. 1·53*a*) and, apart from a small frictional profile drag, exhibit characteristics which are essentially those predicted by perfect fluid theory. For many airfoils this state of affairs continues as α increases until a critical angle of attack is reached at which a separation point suddenly appears on the upper surface near the leading edge (cf. Fig. 1·53*b*). The flow then suddenly changes its character from the streamline to the bluff body type, a large pressure drag is developed, the circulation and lift drop off, and the airfoil is said to have stalled. The angle of attack at which this occurs is sometimes called the "burble point." This rather idealized description is not always applicable, the stall frequently occurring over a small but finite range of α during which the separation point rapidly moves forward without actually jumping to the leading edge. In such cases the drag increase is less precipitous and the peak

of the C_L vs. α curve is rounded instead of having a sharp maximum. The essential physical processes, although more gradual, are still the same.

Phenomena (*a*) to (*c*) of the first paragraph have now been explained. Figure 1·54 gives a schematic summary of some of the more important

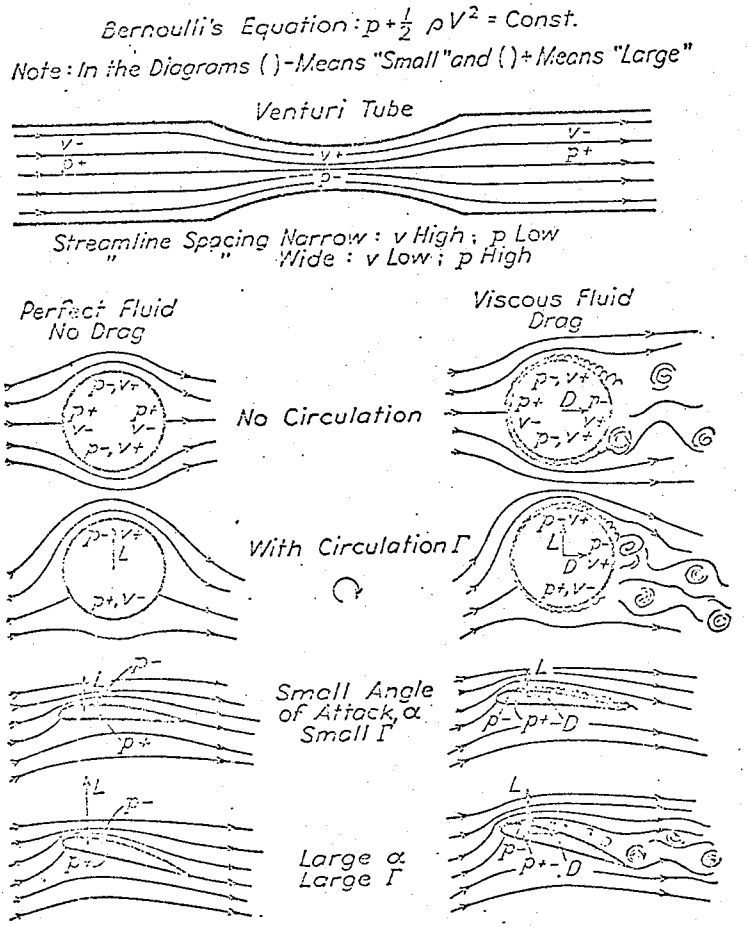

FIG. 1·54. Summary of perfect and real fluid flow characteristics; two-dimensional motion.

flow phenomena in this connection. It only remains in concluding this chapter to complete the physical picture by describing the actual origin and development of the circulation around an airfoil.

It will be remembered that in general the flow without circulation about an airfoil involves flow around the sharp trailing edge. When an

airfoil is set in motion in a stationary fluid this is the type of flow which actually occurs in the first instant as has been repeatedly demonstrated by visual flow observations. The flow around the sharp corner leads to the formation of a vortex as shown in Fig. 1·55.* This is associated

Courtesy of McGraw-Hill Book Co.

FIG. 1·55. Vortex created by flow around a sharp corner.

with the fact that the fluid involved in the formation of the vortex has been in the boundary layer and hence must be considered as a viscous rather than a perfect fluid. As the motion proceeds this vortex is de-

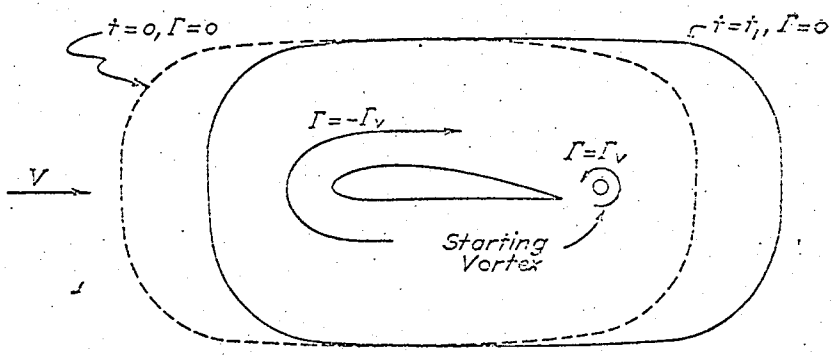

FIG. 1·56. Development of circulation around an airfoil.

tached from the airfoil surface and remains in the fluid behind as a free vortex. At this stage in the proceedings consider a contour surrounding the airfoil and some distance away as indicated in Fig. 1·56. This con-

* Reproduced from Prandtl-Tietjens, *loc. cit.*

tour is attached to a definite set of fluid particles. We adopt the point of view of an observer attached to the airfoil so that we have a rectilinear flow from infinity which suddenly starts from rest. Initially ($t = 0$) everything was at rest so the circulation around the contour was zero. At the later time ($t = t_1$), when the trailing edge vortex has been detached, the contour has moved downstream but is still far from the airfoil so that the fluid particles composing it have not been contaminated by the action of viscosity. In other words, this contour may still be considered as lying in a perfect fluid so that the Thomson theorem of the constancy of circulation (cf. section 1–6) is applicable. Hence the circulation around the contour remains zero at the time t_1. The circulation around any contour is the algebraic sum of all the circulations enclosed by the contour. Now we have at t_1 a circulation, say Γ_v, around the

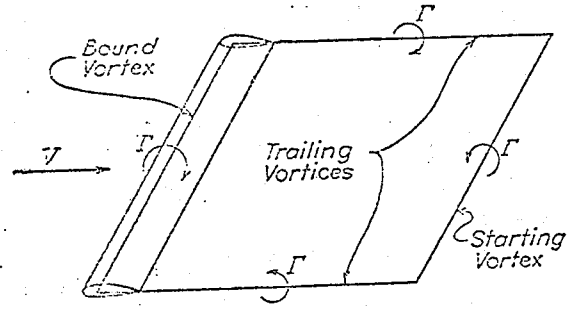

FIG. 1·57. Complete vortex pattern (idealized).

free vortex which has been shed from the trailing edge. In order that the circulation may be zero around the large contour we must also have an equal and opposite circulation, $-\Gamma_v$, which will cancel the Γ_v connected with the starting vortex. This circulation, $-\Gamma_v$, is the airfoil circulation for which we were looking. It is clear that the strength of the "starting vortex," as it is called, will be just such as to make the fluid flow smoothly off the trailing edge, since as long as there is flow around the sharp edge additional starting vortices will be formed which will cause additional circulation around the airfoil and move the rear stagnation point farther aft along the upper surface. Visual flow observations at Prandtl's laboratory show that the above picture is not in the least fictitious but corresponds very closely to the conditions actually observed.

One further remark completes the description of the flow conditions around a finite span wing. From the Helmholtz theorem, stating that vortices cannot end in the fluid, it is at once seen that the starting vortex must actually be connected with the trailing vortices from the wing tips. The final vortex picture is indicated in the sketch of Fig. 1·57. The starting vortex of a wing moving in a stationary fluid is left behind as the wing moves forward, until finally it is so far downstream as to be effectively removed to infinity. This starting vortex formation occurs not only when a wing is first set into motion, but also when the circulation around the wing is subsequently changed for any reason whatever.